

# The relation between $^{13}\text{CO } J=2-1$ line width in molecular clouds and bolometric luminosity of associated IRAS sources

Ke Wang<sup>1</sup>, Yuefang Wu<sup>1</sup>, Liang Ran<sup>1,2</sup>, Wentao Yu<sup>3</sup>, and Martin Miller<sup>4</sup>

<sup>1</sup> Department of Astronomy, School of Physics, Peking University, Beijing 100871, China  
e-mail: kwang@cfa.harvard.edu yfwu@bac.pku.edu.cn

<sup>2</sup> Department of Atmospheric Sciences, School of Physics, Peking University, Beijing 100871, China

<sup>3</sup> Institut für Anorganische Chemie, Universität Bonn, Römer St. 164, D-53117 Bonn, Germany

<sup>4</sup> I. Physikalisches Institut, Universität zu Köln, Zùlpicher St. 77, D-50937 Köln, Germany

Received ?; accepted ?

## ABSTRACT

**Aims.** We search for evidence of a relation between properties of young stellar objects (YSOs) and their parent molecular clouds to understand the initial conditions of high-mass star formation.

**Methods.** A sample of 135 sources was selected from the Infrared Astronomical Satellite (*IRAS*) Point Source Catalog, on the basis of their red color to enhance the possibility of discovering young sources. Using the Kùlner Observatorium für Submillimeter Astronomie (KOSMA) 3-m telescope, a single-point survey in  $^{13}\text{CO } J=2-1$  was carried out for the entire sample, and 14 sources were mapped further. Archival mid-infrared (MIR) data were compared with the  $^{13}\text{CO}$  emissions to identify evolutionary stages of the sources. A  $^{13}\text{CO}$  observed sample was assembled to investigate the correlation between  $^{13}\text{CO}$  line width of the clouds and the luminosity of the associated YSOs.

**Results.** We identified 98 sources suitable for star formation analyses for which relevant parameters were calculated. We detected 18 cores from 14 mapped sources, which were identified with eight pre-UC H II regions and one UC H II region, two high-mass cores earlier than pre-UC H II phase, four possible star forming clusters, and three sourceless cores. By compiling a large (360 sources)  $^{13}\text{CO}$  observed sample, a good correlation was found between the  $^{13}\text{CO}$  line width of the clouds and the bolometric luminosity of the associated YSOs, which can be fitted as a power law,  $\lg(\Delta V_{13}/\text{km s}^{-1}) = (-0.023 \pm 0.044) + (0.135 \pm 0.012) \lg(L_{\text{bol}}/L_{\odot})$ . Results show that luminous ( $> 10^3 L_{\odot}$ ) YSOs tend to be associated with both more massive and more turbulent ( $\Delta V_{13} > 2 \text{ km s}^{-1}$ ) molecular cloud structures.

**Key words.** stars: formation — ISM: clouds — ISM: molecules — ISM: kinematic and dynamics

## 1. Introduction

The past decade has witnessed significant progress in the study of high-mass star formation. Observations at millimeter and submillimeter wavelengths (Zhang et al., 1998; Beuther et al., 2002; Keto, 2002; Zhang, 2005; Cesaroni et al., 2007) suggest that massive proto B stars can form by disk mediated accretion, which is similar to the scenario that produces low-mass stars. However, most of the studies focus on relatively evolved stages, when the central star has already formed and hydrogen burning has begun, characterized by surrounding ultra compact (UC) H II regions and strong emission from complex molecules (Churchwell, 2002). In contrast, the extremely early stages are poorly understood to date. In particular, knowledge to evolutionary stages prior to the onset of H II regions are crucial to understanding the initial conditions of high-mass star formation.

It is known that stars are formed in molecular clouds. Therefore, the relation between forming stars and parent clouds is important to understand the formation process and the properties of the eventual stars. On galaxy scales, star formation activities are usually described by the so-called Schmidt law, which relates the star formation rate (SFR) to the surface density of gas:  $\Sigma_{\text{SFR}} \propto \Sigma_{\text{gas}}^N$ , where the index  $N = 1 - 2$  (Schmidt, 1959; Kennicutt, 1998; Gao & Solomon, 2004). Studies of Galactic dense cores have shown that this relation may be universal and can be connected to Galactic star formation (Wu et al., 2005a).

Larson (1981) studied the turbulence in star forming clouds and found a strong correlation between the internal velocity dispersion  $\sigma$  of the region and its size  $L$ :  $\sigma(\text{km s}^{-1}) \propto L(\text{pc})^{0.38}$ . This relation, also called the Larson law, is valid for low-mass cores but is found to break down in high-mass cores  $\gtrsim 10^3 M_{\odot}$  (Caselli & Myers, 1995; Plume et al., 1997; Guan et al., 2008). This is indicative of the different status of turbulence in low- and high-mass cores. The breakdown of the Larson law can be interpreted as evidence of widespread supersonic turbulence in high-mass cores, in contrast to subsonic turbulent low-mass cores (Plume et al., 1997). A molecular line width is an observational indicator of turbulence in clouds, and bolometric luminosity is an indicator of forming stars. Any relation between these quantities may help us to understand the initial star forming process.

Here we report results from a  $^{13}\text{CO } J=2-1$  survey towards 135 *IRAS* sources using the KOSMA 3-m telescope. To search for high-mass star forming regions in their early stages, we select a sample on the basis of their red *IRAS* color to enhance the possibility of finding young sources. We present the primary results and investigate the relation between line width in molecular clouds and bolometric luminosity of associated infrared sources. We describe our sample selection in Sect. 2 and observations in Sect. 3. In Sect. 4 we present statistical results of the single-point survey (Sect. 4.1) and follow-up mapping (Sect. 4.2). We discuss the  $\Delta V - L$  relation as well as other relations in Sect. 5, and summarize the paper in Sect. 6.

## 2. Sample

We selected the sample from the Infrared Astronomical Satellite (*IRAS*) Point Source Catalog (PSC, Beichman et al. 1988) version 2.1 according to our developed color criteria (Wu et al., 2003), namely:

(a)  $f_{100\mu\text{m}} < 500$  Jy,  $\lg(f_{25\mu\text{m}}/f_{12\mu\text{m}}) \geq 0.7$ ,  $\lg(f_{60\mu\text{m}}/f_{12\mu\text{m}}) \geq 1.4$ , where  $f_\lambda$  is the flux density;

(b) lack of 6 cm radio continuum radiation to exclude potential H II associations;

(c) declination  $\delta > -20^\circ$ , so that targets are accessible to the telescope KOSMA.

Criterion (a) was chosen so that the sample sources were redder and possibly fainter, thus may be younger than those selected based on traditional Wood & Churchwell (1989) color criteria. Criterion (b) helps to exclude any known H II regions brighter than current detection limit. Therefore, the sample should represent extremely young stellar objects (YSOs), mostly at evolutionary stages earlier than the UC H II phase. The 6 cm radio continuum data was extracted from three surveys: (1)  $0^\circ < \delta < 75^\circ$  4.85 GHz radio continuum survey completed by Gregory & Condon (1991) with the 91-m NRAO telescope; (2)  $-29^\circ < \delta < 9.5^\circ$  4.85 GHz radio continuum survey led by Griffith et al. (1994) with the 64-m Parkes telescope; and (3)  $-9.5^\circ < \delta < 10^\circ$  4.85 GHz radio continuum survey led by Griffith et al. (1995) with the 64-m Parkes telescope.

Criteria (a) and (c) lead to 500 sources being selected from the PSC, which contains 245,889 sources. However, only 135 sources were observed because of limited observing time and after applying criterion (b). These sources represent the sample reported in this paper. The sample sources are concentrated across the Galactic plane and cover a wide range of longitude,  $10^\circ < l < 230^\circ$ .

## 3. Observations

A single-point survey in  $^{13}\text{CO } J=2-1$  (220.398 GHz) was carried out from September 2002 to March 2003 using the Kölner Observatorium für Submillimeter Astronomie (KOSMA<sup>1</sup>) 3-m telescope on Gornergrat near Zermatt in Switzerland. All of the sample sources were surveyed in  $^{13}\text{CO } J=2-1$ . About half of the sample sources were also observed in  $^{12}\text{CO } J=2-1$  (230.538 GHz) and 14 of them were mapped in  $^{13}\text{CO } J=2-1$ .

The beamwidth of the KOSMA at 230 GHz was  $130''$ . The pointing accuracy was superior to  $10''$ . The telescope was equipped with a dual-channel SIS receiver, which had a noise temperature of 150 K. A high resolution spectrometer with 2048 channels was employed and the spectral resolution was 165.5 KHz, giving a velocity resolution of  $0.22 \text{ km s}^{-1}$ . The main beam temperature ( $T_{\text{mb}}$ ) had been corrected for the effects of Earth's atmosphere, antenna cover loss, radiation loss, and forward spillover and scattering efficiency (92%). From the calibrated Jupiter observations, the main beam efficiency  $\eta_{\text{mb}}$  was estimated as 68% during our observation. On-the-fly mode was adopted during mapping, with a mapping step of  $60''$ . Most maps were extended until the line intensity decreased to half of the maximum value or even lower. The GILDAS<sup>2</sup> software

<sup>1</sup> The KOSMA 3 m radiotelescope at Gornergrat-Süd Observatory is operated by the University of Cologne and supported by special funding from the Land NRW. The Observatory is administered by the Internationale Stiftung Hochalpine Forschungsstationen Jungfrauoch and Gornergrat, Bern.

<sup>2</sup> available at <http://www.iram.fr/IRAMFR/GILDAS>

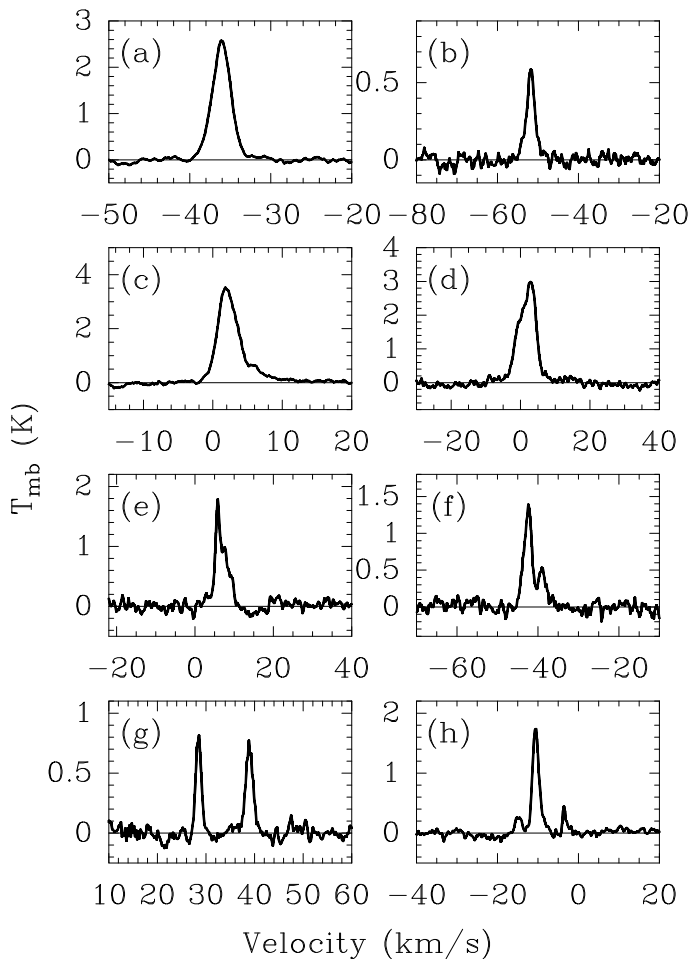


Fig. 1: Example spectra of  $^{13}\text{CO } J=2-1$  towards the *IRAS* sources given in the text.

package (CLASS/GREG/SIC) was used for the data reduction (Guiloteau & Lucas, 2000).

## 4. Results

### 4.1. Survey

Among the entire sample of 135 *IRAS* sources, we identified 98 sources suitable for star formation analyses (another 37 sources were excluded either because they had multiple components or bad baselines, or failed to be detected), of which 60 have both  $^{13}\text{CO } J=2-1$  and  $^{12}\text{CO } J=2-1$  data. Figure 1 presents example spectra of  $^{13}\text{CO } J=2-1$ : (a) *IRAS* 00117+6412, a perfect Gaussian profile; (b) *IRAS* 02541+6208, a fairly narrow line width; (c) *IRAS* 06067+2138, a broad line with red wing, also seen in  $J=1-0$  transition (Wu et al., 2003); (d) *IRAS* 20326+3757, a blue wing; (e) *IRAS* 18278-0212, red asymmetry; (f) *IRAS* 21379+5106, two peaks; (g) *IRAS* 19348+2229, two components; and (h) *IRAS* 02485+6902, multiple components.

Observed and derived parameters are listed in an online Table 1, starting with *IRAS* name and its J2000 equatorial coordinates in Cols. (1) to (3). By Gaussian fit, we obtain the observed parameters including main beam temperature  $T_{\text{mb}}$ , local standard of rest velocity  $V_{\text{LSR}13}$ , and  $^{13}\text{CO } J=2-1$  line width (full width at half-maximum)  $\Delta V_{13}$  for each source, listed in Cols. (4) to (7). When a line profile is obviously non-Gaussian, the pa-

rameters are measured with a cursor (e.g., Wu & Evans 2003), and the velocity uncertainty is given as the velocity resolution; when the line profile has distinctive multiple components, only the strongest component is shown, indicated by a character  $m$  in corresponding  $T_{\text{mb}}$  columns.

The distance to most sources was unavailable in the literature. The kinematic distances were calculated based on the radial velocity  $V_{\text{LSR}13}$  and the velocity field of the outer Galaxy given by Brand & Blitz (1993). When two kinematic distances were available, we selected the closer one, except when the closer distance is too small ( $< 100$  pc). For 8 sources, however, no reasonable distances could be calculated in this way and we assumed that the distance to these sources is 1 kpc. These are marked as \* in the distance Col. (8) of Table 1.

The bolometric luminosity was calculated based on the distances and the *IRAS* fluxes in four bands (12, 25, 60, 100  $\mu\text{m}$ ), following the formula given by Casoli et al. (1986)

$$L_{\text{bol}} = 5.4D^2(f_{12\mu\text{m}}/0.79 + f_{25\mu\text{m}}/2 + f_{60\mu\text{m}}/3.9 + f_{100\mu\text{m}}/9.9) L_{\odot},$$

where  $D$  is the distance in kpc and  $f_{\lambda}$  is the flux density in Jansky. The uncertainties in luminosity originate in the kinematic distances and the quality of the *IRAS* source fluxes. Most of the sample sources have high or moderate quality in all the four bands. Twenty-one sources with upper limit fluxes in one or two bands are marked as  $u$  luminosity in Col. (9) of Table 1.

Assuming local thermodynamic equilibrium (LTE) and that the  $^{13}\text{CO } J=2-1$  transition is optically thin (*i.e.*  $\tau_{13} < 1$ ), we derive excitation temperatures, optical depth and column densities for  $^{13}\text{CO}$ , using radiation transfer equation (Garden et al., 1991). Based on the assumption of LTE,  $^{13}\text{CO}$  and  $^{12}\text{CO}$  share the same excitation temperature  $T_{\text{ex}}$ , which can be derived from the main beam temperature of optically thick  $^{12}\text{CO}$ ,  $T_{\text{mb}12}$ . When  $\tau_{13} > 1$ , an optical depth correction factor  $C_{\tau} = \tau_{13}/(1 - e^{-\tau_{13}})$  is multiplied by its corresponding column density. The relative CO abundance [ $^{12}\text{CO}/\text{H}_2$ ] is estimated to extend from  $2.5 \times 10^{-5}$  (Rodríguez et al., 1982) to  $10^{-4}$  (Garden et al., 1991), and we adopt the median value of  $6.25 \times 10^{-5}$ . Using the terrestrial [ $^{12}\text{C}/^{13}\text{C}$ ] ratio of 89, we adopt a value for [ $^{13}\text{CO}/\text{H}_2$ ] of  $7.0 \times 10^{-7}$  when computing the column density of  $\text{H}_2$ . These parameters are listed in Cols. (10) to (13). References of former works are given in the last Col. (14) of Table 1.

The distribution of  $^{13}\text{CO } J=2-1$  line width of this sample has a mean of  $3.09 \text{ km s}^{-1}$  and a standard deviation of  $1.06 \text{ km s}^{-1}$ . This line width is relatively smaller than that of typical bright/red *IRAS* sources associated with water masers ( $3.5 \text{ km s}^{-1}$ , Wu et al. 2001; note that this value was measured in  $J=1-0$  transition), while significantly larger than that of a molecular cloud hosting intermediate-mass star formation activities ( $\sim 2 \text{ km s}^{-1}$ , Sun et al. 2006, averaged throughout the Perseus cloud). The luminosities are distributed over a wide range, from  $20 L_{\odot}$  to about  $10^5 L_{\odot}$ , with a mean of  $10^4 L_{\odot}$ . The high dispersion of luminosities indicates that these sources are embedded in very different environments. This luminosity distribution is similar to the young 'low' sources of Molinari et al. 1996 (see their Fig. 6), in agreement with the assumption that our sample group may be relatively younger than that chosen by traditional color criteria. The excitation temperature  $T_{\text{ex}}$  ranges from 4.4 to 22.5 K, with an average of 9.7 K. This suggests that very cold gases surround the sample sources, colder than those surrounding the luminous *IRAS* sources (Zhu & Wu, 2007). The  $^{13}\text{CO}$  column densities are  $(1.2 - 28.7) \times 10^{15} \text{ cm}^{-2}$ , with an average of  $6.2 \times 10^{15} \text{ cm}^{-2}$ , while  $\text{H}_2$  column densities are  $(1.7 - 40.8) \times 10^{21} \text{ cm}^{-2}$ , with an average of  $8.9 \times 10^{21} \text{ cm}^{-2}$ . These den-

sities are roughly close to the critical value for gravitational collapse (Hartquist et al., 1998).

#### 4.2. Mapping

To improve our understanding of the properties of the surveyed sample, 14 sources were mapped in  $^{13}\text{CO } J=2-1$  and compared with archival mid-infrared (MIR) continuum data. Mapped sources were selected from the surveyed sample as those with only single emission component, and they almost evenly cover longitude  $70^\circ < l < 230^\circ$ , avoiding low Galactic longitudes, where  $^{13}\text{CO}$  lines are often affected by multiple velocity components from the Galactic molecular ring. Using these sources as a guide, maps were extended until at least one core was resolved. We name a map on the basis of its guide source name, as outlined in Fig. 2. In four cases, one map resolved two cores, resulting in 18 cores in total. We found that 13 cores are associated with the original guide sources, two cores are associated with other *IRAS* sources, and three cores have no embedded infrared source (sourceless hereinafter). A core is named after its associated *IRAS* source; for a sourceless core, it is named after its nearest *IRAS* source plus relative direction to the core (e.g., 20067+3415NE). See Table 2 for core properties.

The core size (Col. 2 of Table 2) is defined as an equivalent linear size  $R = \sqrt{A/\pi}$ , where  $A$  is the projected area of each cloud within the 50% contour (highlighted in Fig. 2). It is corrected for the effect of beam smearing by multiplying its value by a factor  $\sqrt{\theta_{\text{obs}}^2 - \theta_{\text{mb}}^2}/\theta_{\text{obs}}$ , where  $\theta_{\text{obs}}$  is the angular diameter of the core and  $\theta_{\text{mb}}$  is the beamwidth. For three cores, the observed angular diameters are comparable to the beamwidth, so that the cores are just marginally resolved and the corresponding core sizes are highly uncertain. In a few cases, maps were not complete to 50% of the peak intensity, and can only infer lower limits to  $R$  (indicated by a symbol '>'). The average line width of each core (Col. 3) is determined by combining all the spectra in the core and then fitting a Gaussian profile to the average spectrum. In a few cases, the average spectra show line asymmetry/absorption and need to be fitted with two Gaussian profiles, and then the line width of the stronger profile is given. The typical uncertainty in the average line width is  $0.04 \text{ km s}^{-1}$ . Column (4) lists the luminosity also given in Table 1 for reference. Peak volume densities for  $\text{H}_2$ ,  $n(\text{H}_2)$  (Col. 5), and the LTE core masses,  $M_{\text{LTE}}$  (Col. 6), are calculated based on both  $R$  and the peak  $^{13}\text{CO}$  column densities determined by interpolating the maps. For three maps (*IRAS* 06067+2138, 07024-1102, and 21391+5802), however, no  $N(^{13}\text{CO})$  are available in Table 1 because of a lack of  $^{12}\text{CO}$  data. To estimate their core properties, we assume reasonable excitation temperatures: for *IRAS* 06067 and 07024, we assume a typical  $T_{\text{ex}}$  of 15 K; and for *IRAS* 21391, we assume that  $T_{\text{ex}}$  equals the dust temperature (25 K, Beltrán et al. 2002). Column (7) presents the virial mass derived from the sizes and line widths following MacLaren et al. (1988). The ratio of virial to LTE mass  $\alpha = M_{\text{vir}}/M_{\text{LTE}}$  is listed in the last Col. (8) of Table 2. We exclude the marginally resolved cores when computing averages except for the line width column.

Overall, the core mass ranges from  $\sim 10^2 M_{\odot}$  to  $10^4 M_{\odot}$ , the linear size from 0.11 pc to 2.41 pc, and molecular hydrogen density is in the range  $\sim 10^3 - 10^4 \text{ cm}^{-3}$ . The luminosities are once again, distributed across a wide range, from  $30 L_{\odot}$  to  $1.7 \times 10^4 L_{\odot}$ . Overall, the line width  $\overline{\Delta V}_{13} > \sim 2 \text{ km s}^{-1}$ , and has an average of  $2.80 \text{ km s}^{-1}$ , smaller than that of the entire surveyed sample. We find an average value of 1.3 for the ratio of virial to LTE core

Table 2: Core Properties

Core	$R$ (pc)	$\overline{\Delta V}_{13}$ ( $\text{km s}^{-1}$ )	$L_{\text{bol}}$ ( $10^3 L_{\odot}$ )	Peak $n(\text{H}_2)$ ( $10^3 \text{ cm}^{-3}$ )	$M_{\text{LTE}}$ ( $M_{\odot}$ )	$M_{\text{vir}}$ ( $M_{\odot}$ )	$\alpha^*$
(1)	(2)	(3)	(4)	(5)	(6)	(7)	(8)
00117+6412	0.57	2.58	4.29	5.13	1.8E+2	4.8E+2	2.7
00557+5612	1.08	2.05	1.47 <sup>u</sup>	1.66	6.6E+2	5.7E+2	0.9
03101+5821	>1.08	2.52	1.20	1.76	>5.8E+2	8.6E+2	1.5
03260+3111 <sup>a</sup>	>0.23	3.05	0.29	15.96	>1.6E+2	2.6E+2	1.6
03260+3111NE <sup>s</sup>	0.11	2.51	...	15.96	8.0E+1	8.8E+1	1.1
03414+3200	>0.34	1.92	0.05 <sup>u</sup>	5.35	>8.5E+1	1.6E+2	1.8
05168+3634	>2.41	2.86	17.13	1.57	>1.2E+4	2.4E+3	0.2
05168+3634SW <sup>s</sup>	0.60 <sup>m</sup>	2.61	...	1.57	3.0E+3	5.2E+2	0.2
06067+2138	0.55	3.36 <sup>b</sup>	0.03 <sup>u</sup>	3.83 <sup>c</sup>	2.5E+2	7.8E+2	3.1
06103+1523	1.97	2.56	9.49	1.02	2.8E+3	1.6E+3	0.6
07024-1102	>0.11 <sup>m</sup>	1.99	0.57	64.73 <sup>c</sup>	>9.0E+0	5.8E+1	6.4
20067+3415	1.76	3.80 <sup>b</sup>	1.14	1.14	3.9E+3	3.2E+3	0.8
20067+3415NE <sup>s</sup>	0.45 <sup>m</sup>	3.67	...	1.14	9.7E+2	7.5E+2	0.8
20149+3913	0.43	3.19	0.30 <sup>u</sup>	2.62	1.4E+3	5.5E+2	0.4
20151+3911 <sup>a</sup>	>1.30	3.83	0.70 <sup>u</sup>	2.62	>4.1E+3	2.4E+3	0.6
21391+5802	0.32	2.78	0.26	11.87 <sup>c</sup>	1.3E+2	3.1E+2	2.4
22198+6336	1.22	2.21 <sup>b</sup>	1.53 <sup>u</sup>	2.39	1.7E+3	7.5E+2	0.4
22506+5944	1.31	2.88	6.83	1.40	1.0E+3	1.4E+3	1.4
Average <sup>†</sup>	0.98	2.80	3.02	4.95	1.9E+3	1.1E+3	1.3

Note.— <sup>a</sup> not guide *IRAS* source. Luminosity calculated based on *IRAS* fluxes and distance: 03260+3111 at 0.4 kpc (Harju et al., 1998) and 20151+3911 at 1.7 kpc (Motte et al., 2007). <sup>b</sup> average spectrum fitted with two Gaussian profiles, list the stronger one. <sup>c</sup> no <sup>12</sup>CO data, density calculated by assuming reasonable  $T_{\text{ex}}$  (see text). <sup>m</sup> core's angular diameter comparable to beamwidth, marginally resolved. <sup>s</sup> sourceless core. <sup>u</sup> upper limit. <sup>†</sup> average calculating does not include values of marginally resolved cores, except for the line width column. \*  $\alpha = M_{\text{vir}}/M_{\text{LTE}}$ .

mass,  $\alpha$ . Overall the mapping sample infers  $\alpha \sim 1$ , indicating that most of the cores appear to be virialized.

Comparisons between <sup>13</sup>CO maps and MIR images are presented in Fig. 2, and a detailed evolutionary identification of individual mapped sources is presented in the online Appendix A.

## 5. Discussion

### 5.1. The line width-luminosity relation

The empirical correlation of line width versus luminosity has been found by various authors from observations in C<sup>18</sup>O (Saito et al., 2001; Ridge et al., 2003), as well as in NH<sub>3</sub> (Wouterloot et al., 1988; Myers et al., 1991; Harju et al., 1993; Ladd et al., 1994; Jijina et al., 1999). The line width is in general found to increase with luminosity, for different  $\lg(\Delta V)/\lg(L_{\text{bol}})$  slopes: 0.13-0.19 for NH<sub>3</sub> (Jijina et al., 1999) and 0.11 for C<sup>18</sup>O (Saito et al., 2001). Given the relatively wide availability of the archival <sup>13</sup>CO data, it is helpful to compile an up-to-date <sup>13</sup>CO observed sample to investigate the luminosity-line width relation in case of <sup>13</sup>CO.

In Fig. 3, we plot in logarithmic space the line width versus luminosity from our sample and other <sup>13</sup>CO observed samples adopted from the literature (Beichman et al., 1986; Dent et al., 1985; Fischer et al., 1985; Yamashita et al., 1989; Wu et al., 2001, 2004; Ridge et al., 2003). This sample contains 360 sources in total. One finds that the luminosity of the *IRAS* sources is well correlated with the <sup>13</sup>CO line width, as fitted by a power law:

$$\lg\left(\frac{\Delta V_{13}}{\text{km s}^{-1}}\right) = (-0.023 \pm 0.044) + (0.135 \pm 0.012) \lg\left(\frac{L_{\text{bol}}}{L_{\odot}}\right),$$

where the correlation coefficient c.c. = 0.69. This suggests that the mass of the forming stellar objects is linked to the dynamic

status of their parent clouds. Saito et al. (2001) measured a similar correlation in the Centaurus tangential region and suggested that the mass of the formed stars is determined by the internal velocity dispersion of the dense cores. If the velocity dispersion is a reliable indicator of the turbulence, this is consistent with the idea that turbulence is different in high-mass and low-mass cores. We note that the <sup>13</sup>CO line widths adopted from the literature were measured from  $J = 1 - 0$  transition with smaller beams.

It is generally agreed that embedded infrared point sources of high luminosity ( $\geq 10^3 L_{\odot}$ ) but without associated H II regions are good candidates to be high-mass YSOs in the pre-UC H II phase (e.g., Wu et al. 2006 and references therein). However, sufficiently young massive objects are not necessarily bright at infrared wavelengths; some of them have no infrared counterparts. High-mass objects at sufficiently young evolutionary stages could be quite faint in infrared ranges either because they are not yet mature enough to have developed infrared emission or they are embedded very deeply in cold dust. For instance, Sridharan et al. (2005) identified several 1.2 mm emitting high-mass starless cores (HMSCs) that exhibit absorption or no emission at the MIR wavelengths; a centimeter-emitting UC H II region was also found without an infrared counterpart (Forbrich et al., 2008). In our mapped sample, faint ( $< 10^3 L_{\odot}$ ) sources associated with very massive ( $> 10^3 M_{\odot}$ ) cores (20149, 20151) do exist. Although we cannot rule out the possibility that these two sources could evolve to only low-mass stars, it is very likely that the clouds will eventually fragment to form high-mass stars, given the large amount of gas therein.

Hereafter, for clarity, our *luminosity criterion* refers to bolometric luminosity  $L_{\text{bol}} \geq 10^3 L_{\odot}$ , and our *line-width criterion* refers to line width  $\Delta V(^{13}\text{CO } J=2-1) > 2 \text{ km s}^{-1}$ . According to the  $\Delta V - L$  relation above, luminosity  $L_{\text{bol}} = 10^3 L_{\odot}$  corresponds to  $\Delta V_{13} = 2.42^{+0.49}_{-0.41} \text{ km s}^{-1}$ . Because high-mass stars

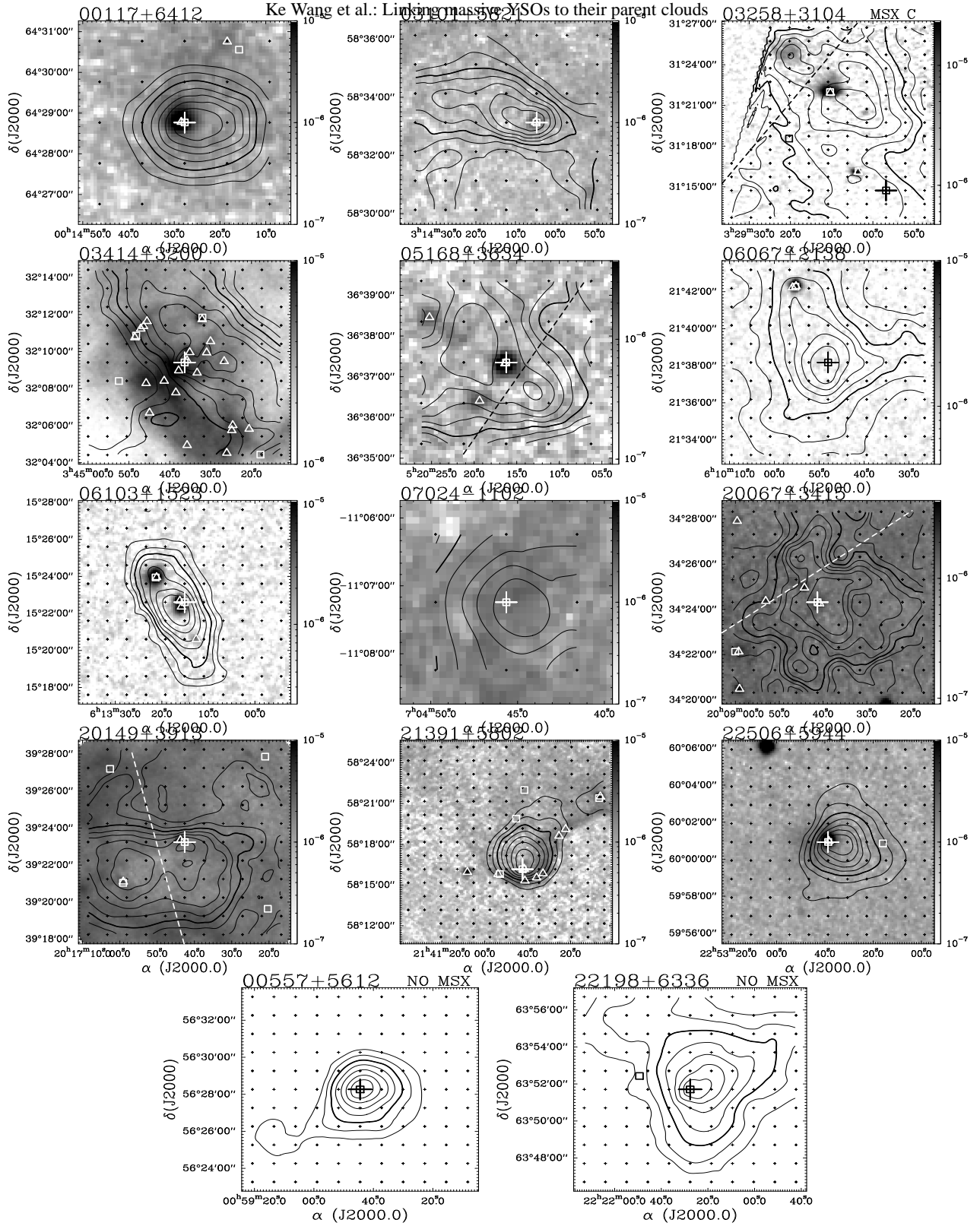


Fig. 2:  $^{13}\text{CO } J=2-1$  integrated intensity contours overlay the *Midcourse Space Experiment* (*MSX*; Price et al. 2001) band A ( $8.28 \mu\text{m}$ ) images as background, if available. Maps are listed in order of name, except the two without *MSX* data. *IRAS* 03258+3104 has no band A data and we use band C instead; *IRAS* 00557+5612 and 22198+6336 both have no *MSX* data available, as labeled on the top of their relevant sub-figures. *IRAS* point sources are denoted by squares while *MSX* point sources by triangles. Small crosses represent observed points, while large crosses denote the original guide sources (Sect. 4.2), as labeled on the top of each map. Dash lines schematically separate resolved cores. For integration, only intensity over three times of the standard deviation ( $3\sigma$ ) is considered. Contour levels begin from 30% to 90% by 10% of the peak intensity, while 50% level is highlighted by a solid thick contour. For *MSX* images, the grey scale wedge is shown on the right side; the unit is  $\text{W m}^{-2} \text{sr}^{-1}$ .

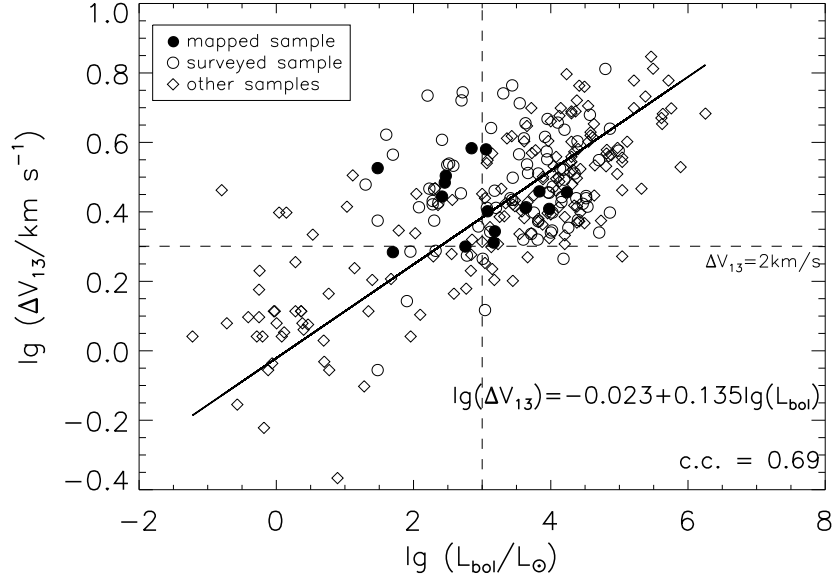


Fig. 3: Line width plotted versus bolometric luminosity of 360  $^{13}\text{CO}$  observed sources: surveyed sources (open circles), mapped sources (filled circles), and other samples adopted from the literature (diamonds). Solid line represents a least squares fitting to the data, and the dash lines represent the luminosity/line-width criteria (Sect. 5.1).

are far more luminous than their low-mass counterparts, luminous *IRAS* sources ( $\geq 10^3 L_{\odot}$ ) are likely to be high-mass stellar objects. Therefore, we tentatively (not exclusively) suggest the lower limit,  $\Delta V_{13} = 2 \text{ km s}^{-1}$ , as a characteristic value for the line-width criterion, analogous to the widely used luminosity criterion. Objects with line width larger than this characteristic value are probably high-mass objects. The line-width criterion includes 94.5% sources that also satisfy the luminosity criterion (Fig. 3), which implies that line width may be a key parameter in measuring the masses of the forming stellar objects in the cores, at least in our sample. We note that this criterion ( $2 \text{ km s}^{-1}$ ) is larger than the typical line width of low mass cores ( $1.3 \text{ km s}^{-1}$ , Myers et al. 1983), and smaller than the average line width of high-mass cores ( $3.5 \text{ km s}^{-1}$ , Wu et al. 2001).

Applying the luminosity/line-width criteria to our sample, there are 68 sources satisfying luminosity criterion, 65 (95.6%) of which also satisfy line-width criterion. We suggest that the 65 sources are candidate high-mass star formation regions in a pre-UC H II phase. For the remaining 30 less luminous sources, 23 of them satisfy the line-width criterion but not the luminosity criterion. We suggest that the 23 sources are high-mass YSO candidates earlier than pre-UC H II phase.

## 5.2. Core masses and line widths

The core masses provide a direct test of our line-width criterion. Figure 3 includes 15 cores with luminosities listed in Table 2. We exclude sourceless cores and marginally resolved cores in the discussion in this section, because the former's luminosity cannot be determined and latter's estimated size and mass are highly uncertain. The remaining 14 luminosity-available cores can be divided into two groups: Group I, which do not satisfy the luminosity criterion, including 03414, 21391, 03260, 20149, 06067, 20151; and group II, satisfying the luminosity criterion, including 00557, 22198, 03101, 06103, 00117, 05168, 22506, 20067 (in order of increasing line width). All group II cores

also satisfy the line-width criterion, and they are located in the upper right panel of Fig. 3. They are very massive, their estimated masses being higher than several  $10^2 M_{\odot}$ , except core 00117 ( $1.8 \times 10^2 M_{\odot}$ ). On the other hand, group I cores mostly satisfy the line-width criterion. They are relatively less massive than group II cores, their masses being typically  $\sim 10^2 M_{\odot}$  or more, with two very massive cores 20149 and 20151 ( $> 10^3 M_{\odot}$ ). The only case that does not satisfy the line-width criterion, core 03414, has the lowest mass in group I. We note that all group I cores are still significantly more massive than the low-mass cores (Myers et al., 1983).

The high-mass nature of group I cores confirms again (in addition to the previously mentioned cores 20149, 20151) that the luminosity criterion cannot be applied to some young sources. On the other hand, the line-width criterion is applicable to our sample. While in terms of inferring mass, line width may not be as direct an indicator as luminosity, it is helpful when luminosity is unavailable or is affected by large uncertainty (e.g., due to distance ambiguity, flux upper limit), which is often the case. In addition, line width can be measured observationally more easily and more accurately than luminosity.

In Fig. 4 (a), we plot  $\lg(\Delta V_{13})$  versus  $\lg M_{\text{LTE}}$ . A weak correlation is evident in the data, with a correlation coefficient of 0.38. This may indicate that, for molecular clouds with associated YSOs, the  $^{13}\text{CO}$  line width at some degree is related to the cloud mass, and massive cores tend to have larger line widths. This weak correlation, together with the strong  $\Delta V - L$  correlation, indicates that massive stars are more likely to form in massive molecular cores. The core mass and associated *IRAS* luminosity in our mapped sample are indeed well correlated (c.c. = 0.76). However, this correlation may need to be corrected for distance effects (0.3–6.08 kpc for mapped sample) because both mass and luminosity are proportional to  $D^2$ . Nevertheless, strong mass-luminosity correlations were reported in other regions or samples that have far smaller distance differences than our sample (Dobashi et al., 1996; Saito et al., 2001; Ridge et al.,

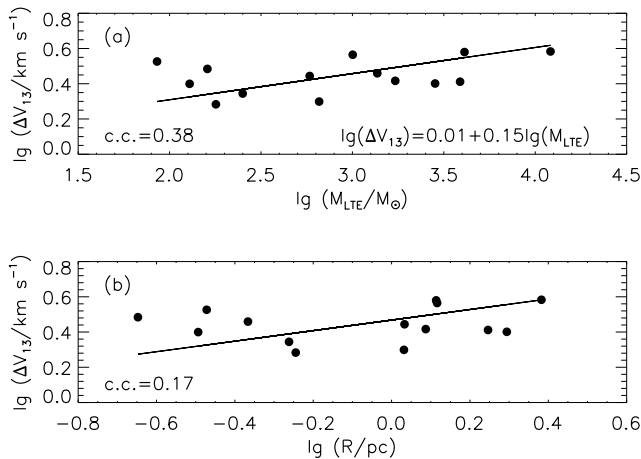


Fig. 4: Relations between  $^{13}\text{CO}$  line width  $\Delta V_{13}$  and other physical parameters of molecular cores: (a) LTE mass  $M_{\text{LTE}}$ , and (b) size  $R$ . In both cases, the filled circles represent data and solid lines are linear fitting results to the data. The fitting function and correlation coefficient are labeled in each panel.

2003). Figure 4 (b) plots line width  $\Delta V_{13}$  and core size  $R$  in logarithm. With an average virial mass of  $1.1 \times 10^3 M_{\odot}$ , the cores exhibit no correlation between size and line width. This indicates that the Larson law is invalid for our mapped sample, consistent with the results of previous works (Plume et al. 1997,  $\langle M_{\text{vir}} \rangle > 3.8 \times 10^3 M_{\odot}$ ; Guan et al. 2008,  $\langle M_{\text{vir}} \rangle = 5.6 \times 10^3 M_{\odot}$ ). The correlations in Fig. 4 are unaffected by distance, because the line width and distance of the plotted cores are not correlated (c.c. = 0.04).

We conclude that, based on the currently available sample, YSOs with higher bolometric luminosity ( $> 10^3 L_{\odot}$ ), tend to be associated with more massive molecular cloud structures, which are usually more turbulent, and have a large  $^{13}\text{CO}$  line width,  $\Delta V_{13} > 2 \text{ km s}^{-1}$ . It is important to note that, the characteristic value ( $2 \text{ km s}^{-1}$ ) may not be universal, and can vary from region to region and/or from line to line. Further mapping of more clouds, as well as higher angular resolution data if available, are required to examine the line-width criterion proposed here.

## 6. Summary

We have carried out a  $^{13}\text{CO } J=2-1$  survey of 135 *IRAS* sources selected as potential YSOs earlier than UC H II regions. Our main findings are summarized as follows:

1. Ninety-eight sources have good enough emission profile for analysis; some of them show asymmetric line profiles of  $^{13}\text{CO } J=2-1$ . The line width is  $3.09 \text{ km s}^{-1}$  and excitation temperature is  $9.7 \text{ K}$ , on average. The  $\text{H}_2$  column densities are  $(1.7 - 40.8) \times 10^{21} \text{ cm}^{-2}$ . Sixty-five sources are suggested to be candidate precursors of UC H II regions.

2. Fourteen sources were mapped and resolved as eighteen cores, which have been identified with eight pre-UC H II regions and one UC H II region, two high-mass cores earlier than pre-UC H II phase, four possible star forming clusters, and three source-less cores.

3. For molecular clouds with known associated YSOs and measured  $L_{\text{bol}}$ ,  $^{13}\text{CO}$  line width  $\Delta V_{13}$  of the clouds is correlated with the bolometric luminosity of the YSOs. Based on the current  $^{13}\text{CO}$  observed sample (360 sources in total), this

correlation can be fitted as a power law,  $\lg(\Delta V_{13} / \text{km s}^{-1}) = (-0.023 \pm 0.044) + (0.135 \pm 0.012) \lg(L_{\text{bol}}/L_{\odot})$ .

4. Luminous ( $> 10^3 L_{\odot}$ ) YSOs tend to be produced in more massive and more turbulent ( $\Delta V_{13} > 2 \text{ km s}^{-1}$ ) molecular cloud structures.

5. High-mass stars are more likely to form in massive molecular clouds.

*Acknowledgements.* We are grateful to Q. Zhang, X. Guan, R. Xue and L. Zhu for valuable discussion. We thank H. Du and F. Virgili for their help on the manuscript. We also thank the anonymous referee whose comments and suggestions helped to improve the content and the clarity of this paper. This research is supported by Grants 10733030 and 10873019 of NSFC. It made use of data products from the Infrared Astronomical Satellite (*IRAS*) and the Midcourse Space Experiment (*MSX*) retrieved from the NASA/IPAC Infrared Science Archive, which is operated by the JPL/Caltech under a contract with NASA.

## References

- Ao, Y., Yang, J., & Sunada, K. 2004, *AJ*, 128, 1716  
 Beichman, C. A., Myers, P. C., Emerson, J. P., et al. 1986, *ApJ*, 307, 337  
 Beichman, C. A., Neugebauer, G., Habing, H. J., Clegg, P. E., & Chester, T. J., eds. 1988, *Infrared astronomical satellite (IRAS) catalogs and atlases. Volume 1: Explanatory supplement, Vol. 1*  
 Beltrán, M. T., Girart, J. M., Estalella, R., Ho, P. T. P., & Palau, A. 2002, *ApJ*, 573, 246  
 Beuther, H., Schilke, P., Sridharan, T. K., et al. 2002, *A&A*, 383, 892  
 Brand, J. & Blitz, L. 1993, *A&A*, 275, 67  
 Brand, J., Cesaroni, R., Caselli, P., et al. 1994, *A&AS*, 103, 541  
 Bronfman, L., Nyman, L.-A., & May, J. 1996, *A&AS*, 115, 81  
 Caselli, P. & Myers, P. C. 1995, *ApJ*, 446, 665  
 Casoli, F., Combes, F., Dupraz, C., Gerin, M., & Boulanger, F. 1986, *A&A*, 169, 281  
 Cesaroni, R., Galli, D., Lodato, G., Walmsley, C. M., & Zhang, Q. 2007, in *Protostars and Planets V*, ed. B. Reipurth, D. Jewitt, & K. Keil, 197–212  
 Churchwell, E. 2002, *ARA&A*, 40, 27  
 Churchwell, E., Walmsley, C. M., & Cesaroni, R. 1990, *A&AS*, 83, 119  
 Dent, W. R. F., Little, L. T., Kaifu, N., Ohishi, M., & Suzuki, S. 1985, *A&A*, 146, 375  
 Dobashi, K., Bernard, J.-P., & Fukui, Y. 1996, *ApJ*, 466, 282  
 Fischer, J., Sanders, D. B., Simon, M., & Solomon, P. M. 1985, *ApJ*, 293, 508  
 Forbrich, J., Menten, K. M., & Reid, M. J. 2008, *A&A*, 477, 267  
 Gao, Y. & Solomon, P. M. 2004, *ApJ*, 606, 271  
 Garden, R. P., Hayashi, M., Hasegawa, T., Gatley, I., & Kaifu, N. 1991, *ApJ*, 374, 540  
 Gregory, P. C. & Condon, J. J. 1991, *ApJS*, 75, 1011  
 Griffith, M. R., Wright, A. E., Burke, B. F., & Ekers, R. D. 1994, *ApJS*, 90, 179  
 Griffith, M. R., Wright, A. E., Burke, B. F., & Ekers, R. D. 1995, *ApJS*, 97, 347  
 Guan, X., Wu, Y., & Ju, B. 2008, *MNRAS*, 391, 869  
 Guilloteau, S. & Lucas, R. 2000, in *Astronomical Society of the Pacific Conference Series, Vol. 217, Imaging at Radio through Submillimeter Wavelengths*, ed. J. G. Mangum & S. J. E. Radford, 299  
 Harju, J., Lehtinen, K., Booth, R. S., & Zinchenko, I. 1998, *A&AS*, 132, 211  
 Harju, J., Walmsley, C. M., & Wouterloot, J. G. A. 1993, *A&AS*, 98, 51  
 Hartquist, T. W., Caselli, P., Rawlings, J. M. C., Ruffle, D. P., & Williams, D. A. 1998, in *The Molecular Astrophysics of Stars and Galaxies*, ed. T. W. Hartquist & D. A. Williams, 101  
 Jijina, J., Myers, P. C., & Adams, F. C. 1999, *ApJS*, 125, 161  
 Kennicutt, Jr., R. C. 1998, *ApJ*, 498, 541  
 Keto, E. 2002, *ApJ*, 568, 754  
 Kim, K.-T. & Kurtz, S. E. 2006, *ApJ*, 643, 978  
 Knee, L. B. G. & Sandell, G. 2000, *A&A*, 361, 671  
 Ladd, E. F., Myers, P. C., & Goodman, A. A. 1994, *ApJ*, 433, 117  
 Larson, R. B. 1981, *MNRAS*, 194, 809  
 Lee, Y. & Jung, J.-H. 2003, *New Astronomy*, 8, 191  
 MacLaren, I., Richardson, K. M., & Wolfendale, A. W. 1988, *ApJ*, 333, 821  
 Matthews, H. I. 1979, *A&A*, 75, 345  
 Molinari, S., Brand, J., Cesaroni, R., & Palla, F. 1996, *A&A*, 308, 573  
 Motte, F., Bontemps, S., Schilke, P., et al. 2007, *A&A*, 476, 1243  
 Myers, P. C., Ladd, E. F., & Fuller, G. A. 1991, *ApJ*, 372, L95  
 Myers, P. C., Linke, R. A., & Benson, P. J. 1983, *ApJ*, 264, 517  
 Palla, F., Brand, J., Comoretto, G., Felli, M., & Cesaroni, R. 1991, *A&A*, 246, 249  
 Plume, R., Jaffe, D. T., Evans, II, N. J., Martin-Pintado, J., & Gomez-Gonzalez, J. 1997, *ApJ*, 476, 730

- Price, S. D., Egan, M. P., Carey, S. J., Mizuno, D. R., & Kuchar, T. A. 2001, *AJ*, 121, 2819
- Richards, P. J., Little, L. T., Heaton, B. D., & Toriseva, M. 1987, *MNRAS*, 228, 43
- Ridge, N. A., Wilson, T. L., Megeath, S. T., Allen, L. E., & Myers, P. C. 2003, *AJ*, 126, 286
- Rodriguez, L. F., Carral, P., Ho, P. T. P., & Moran, J. M. 1982, *ApJ*, 260, 635
- Saito, H., Mizuno, N., Moriguchi, Y., et al. 2001, *PASJ*, 53, 1037
- Schmidt, M. 1959, *ApJ*, 129, 243
- Sridharan, T. K., Beuther, H., Saito, M., Wyrowski, F., & Schilke, P. 2005, *ApJ*, 634, L57
- Sun, K., Kramer, C., Ossenkopf, V., et al. 2006, *A&A*, 451, 539
- Szymczak, M., Hrynek, G., & Kus, A. J. 2000, *A&AS*, 143, 269
- Wood, D. O. S. & Churchwell, E. 1989, *ApJ*, 340, 265
- Wouterloot, J. G. A., Brand, J., & Fiegle, K. 1993, *A&AS*, 98, 589
- Wouterloot, J. G. A., Walmsley, C. M., & Henkel, C. 1988, *A&A*, 203, 367
- Wu, J. & Evans, II, N. J. 2003, *ApJ*, 592, L79
- Wu, J., Evans, II, N. J., Gao, Y., et al. 2005a, *ApJ*, 635, L173
- Wu, Y., Wang, J., & Wu, J. 2003, *Chinese Physics Letters*, 20, 1409
- Wu, Y., Wei, Y., Zhao, M., et al. 2004, *A&A*, 426, 503
- Wu, Y., Wu, J., & Wang, J. 2001, *A&A*, 380, 665
- Wu, Y., Zhang, Q., Chen, H., et al. 2005b, *AJ*, 129, 330
- Wu, Y., Zhang, Q., Yu, W., et al. 2006, *A&A*, 450, 607
- Yamashita, T., Suzuki, H., Kaifu, N., et al. 1989, *ApJ*, 347, 894
- Zhang, Q. 2005, in *IAU Symposium*, Vol. 227, *Massive Star Birth: A Crossroads of Astrophysics*, ed. R. Cesaroni, M. Felli, E. Churchwell, & M. Walmsley, 135–144
- Zhang, Q., Hunter, T. R., Brand, J., et al. 2005, *ApJ*, 625, 864
- Zhang, Q., Hunter, T. R., & Sridharan, T. K. 1998, *ApJ*, 505, L151
- Zhao, M., Wu, Y., Miller, M., & Mao, R. 2003, *Acta Astronomica Sinica*, 44, 103
- Zhu, L. & Wu, Y.-F. 2007, *Chinese Journal of Astronomy and Astrophysics*, 7, 331



## Appendix A: Individual Analyses

In Fig. 2, we compare the integrated intensity of  $^{13}\text{CO}$  emissions to *IRAS* (point sources) and *MSX* (point sources and images) data. We use the most sensitive band (band A, centered on  $8.28\ \mu\text{m}$ ) images of *MSX* when available. We note that maps in Fig. 2 are labeled by the original guide sources (Sect. 4.2). *IRAS* 03258+3104 has no band A data and we use band C (centered on  $12.13\ \mu\text{m}$ ) instead. *IRAS* 00557+5612 and 22198+6336 both have no *MSX* data. Individual analyses of each map are presented as follows.

*IRAS 00117+6412*:  $^{13}\text{CO}$  emission peak coincides well with *IRAS* and *MSX* point sources, and there are also strong counterparts in all four *MSX* bands. This distinctive  $^{13}\text{CO}$  core is massive ( $1.8 \times 10^2 M_\odot$ ), in agreement with the conclusion deduced from the luminosity/line-width criteria (Sect. 5.1). We therefore suggest that it is a pre-UC H II region. Strong 22 GHz water maser (Wouterloot et al., 1993) and outflow activity (Zhang et al., 2005; Zhao et al., 2003) have been detected within this area, providing evidence of active star formation.

*IRAS 00557+5612*: *MSX* data are unavailable close to this region, but the *IRAS* source matches well to the  $^{13}\text{CO}$  core peak. A core as massive as  $6.6 \times 10^2 M_\odot$  agrees with the conclusion deduced from the luminosity/line-width criteria. We therefore suggest that it is a pre-UC H II region. A velocity gradient of  $0.36\ \text{km s}^{-1}\ \text{pc}^{-1}$  from northeast to southwest is inferred, yielding a rotating angular velocity of  $1.16 \times 10^{-14}\ \text{s}^{-1}$ . According to  $^{13}\text{CO}\ J=1-0$  and  $\text{HCO}^+$  mapping by Zhu & Wu (2007), two subcores exist within this core.

*IRAS 03101+5821*:  $^{13}\text{CO}$  emission coincides with infrared point sources and image as well. A core more massive than  $5.8 \times 10^2 M_\odot$  agrees with the conclusion drawn from the luminosity/line-width criteria. We therefore suggest that it is a pre-UC H II region. A 22 GHz water maser has been detected within this area (Wouterloot et al., 1993).

*IRAS 03258+3104*: a *MSX* band A image is unavailable for this region and we use band C instead.  $^{13}\text{CO}$  emission within this area is more diffuse than that in former sources. At least two cores (03260+3111 and 03260+3111NE) are resolved within an area of 0.34 pc. The larger core coincides with *IRAS* 03260+3111, which does not satisfy our color selection criteria and was suggested as an UC H II region by Churchwell et al. (1990). Taking both their line width and luminosity into account, we suggest that core 03260+3111 is a high-mass object in UC H II phase, while 03260+3111NE is a sourceless core. The original guide source of the map, *IRAS* 03258+3104, is not associated with any resolved  $^{13}\text{CO}$  core. It has been suggested to be a Class 0 object driving a low-mass bipolar CO outflow (Knee & Sandell, 2000).

*IRAS 03414+3200*:  $^{13}\text{CO}$  is quite diffuse across the entire area of 0.34 pc, so that no distinctive  $^{13}\text{CO}$  core is found. However, several infrared point sources are evident close to the 90% contour within one beam, superimposed on a steep density gradient. Although its mass ( $> 85 M_\odot$ ) and line width ( $1.92\ \text{km s}^{-1}$ ) are relatively low in all the mapped sources, it appears to be a star forming cluster.

*IRAS 05168+3634*: at least two cores (05168+3634 and 05168+3634SW) are present within 3.01 pc. The dominant

northeastern core appears to be associated with the infrared sources. The total core mass higher than  $1.5 \times 10^4 M_\odot$  agrees with the conclusion deduced from the luminosity/line-width criteria. We suggest that the dominant core is a high-mass star forming region in pre-UC H II phase, and the SW core is a sourceless core. This is consistent with results from Molinari et al. (1996). Strong outflow activity was identified (Brand et al., 1994; Zhang et al., 2005) at the position of the NE core, and the outflow driving source appears deviated to the infrared source *IRAS* 05168+3634. A 22 GHz water maser was detected by Palla et al. (1991) in this region.

*IRAS 06067+2138*:  $^{13}\text{CO}$  core coincides with the *IRAS* point source but is without *MSX* counterpart. The core mass  $M_{\text{LTE}}$  ( $2.5 \times 10^2 M_\odot$ ) is only one third of its virial mass  $M_{\text{vir}}$  ( $7.8 \times 10^2 M_\odot$ ), indicating that the core is not yet gravitationally bound. Taking its large line width ( $3.36\ \text{km s}^{-1}$ ) into account, we suggest that it is a high-mass object earlier than pre-UC H II phase.

*IRAS 06103+1523*:  $^{13}\text{CO}$  emission coincides with both infrared point sources and image. A core as massive as  $2.8 \times 10^3 M_\odot$  agrees with the conclusion deduced from the luminosity/line-width criteria. *IRAS* 06103+1523 is found to be two point sources by *MSX* data, implying that a fine structure may exist there. A denser molecular tracer (e.g.,  $\text{N}_2\text{H}^+$  or  $\text{HCO}^+$ ) and a higher resolution (several arcsec) are needed to study these fine structures. We therefore suggest that it is a high-mass star forming cluster.

*IRAS 07024-1102*:  $^{13}\text{CO}$  map is incomplete but a core is clearly evident. The core coincides with the *IRAS* point source but does not have a *MSX* counterpart. Although its luminosity ( $570 L_\odot$ ) is a little lower than the luminosity criterion, it does generate a line width ( $1.99\ \text{km s}^{-1}$ ) very close to the line-width criterion. We therefore suggest that it is a high-mass object earlier than pre-UC H II phase.

*IRAS 20067+3415*: the  $^{13}\text{CO}$  gas distribution is quite complex in this region. At least two cores (20067+3415 and 20067+3415NE) are revealed. The dominant southwestern core coincides with infrared point sources, while the northeastern core is a sourceless core. Several sub-structures are revealed within an area of 2.21 pc with total mass of  $4.9 \times 10^3 M_\odot$ . Thus, we suggest that core 20067+3415 is a high-mass star forming cluster. The MIR emission and luminosity are relatively weak compared to those of other pre-UC H II regions, indicating a very early evolutionary stage.

*IRAS 20149+3913*:  $^{13}\text{CO}$  emission reveals two cores (20149+3913 and 20151+3911); both also coincide with infrared point sources and image. They do not satisfy the luminosity criterion but have large line widths, consistent with their high masses. Both sources are located in the Cygnus X molecular cloud complex and were mapped in 1.2 mm continuum (Motte et al., 2007), yielding masses  $8 M_\odot$  and  $23 M_\odot$ , respectively (see their Table 1 and Fig. 13). Here we suggest that both cores are pre-UC H II regions.

*IRAS 21391+5802*:  $^{13}\text{CO}$  emission detects a distinctive core and a belt of gas distributed along the southeast to northwest direction, which is coincident with the MIR background and several point sources. The core mass  $M_{\text{LTE}}$  ( $1.3 \times 10^2 M_\odot$ ) is roughly half of its virial mass  $M_{\text{vir}}$  ( $3.1 \times 10^2 M_\odot$ ), indicating

that the core is not yet gravitationally bound, responsible for a large line width ( $2.78 \text{ km s}^{-1}$ ). Taking its relatively small size ( $0.32 \text{ pc}$ ) into account, we suggest that it is a star forming cluster where high-mass stars could eventually form. A 22 GHz water maser and outflow were identified in this region (Palla et al., 1991; Zhang et al., 2005).

*IRAS 22198+6336*: *MSX* data are unavailable near this region, but the *IRAS* source matches the  $^{13}\text{CO}$  core peak well. A core as massive as  $1.7 \times 10^3 M_{\odot}$  agrees with the conclusion deduced from the luminosity/line-width criteria. A 22 GHz water maser and outflow were identified in this region (Palla et al., 1991; Zhang et al., 2005). We therefore suggest that it is a pre-UC H II region.

*IRAS 22506+5944*:  $^{13}\text{CO}$  core coincides well with a luminous *IRAS* point source and a bright *MSX* counterpart. A core as massive as  $1.0 \times 10^3 M_{\odot}$  agrees with the conclusion deduced from the luminosity/line-width criteria. Thus, we suggest that it is a pre-UC H II region. Outflow activity (Wu et al., 2005b; Zhang et al., 2005) and a 22 GHz water maser (Palla et al., 1991) were identified, indicating that active star formation process is underway.

In summary,  $^{13}\text{CO } J=2-1$  mapping reveals at least 18 massive cores from 14 maps. By means of individual analyses, we identify eight pre-UC H II regions and one UC H II region, two high-mass cores earlier than pre-UC H II phase, four possible star forming clusters, and three sourceless cores.

Table 1: Observed and Derived Parameters of Surveyed Sources

Source	Observed Parameters						Derived Parameters						
	$\alpha$ (J2000) (h m s)	$\delta$ (J2000) ( $^{\circ}$ ' '')	$T_{\text{mb}12}$ (K)	$T_{\text{mb}13}$ (K)	$V_{\text{LSR}13}$ (km s $^{-1}$ )	$\Delta V_{13}$ (km s $^{-1}$ )	$D$ (kpc)	$L_{\text{bol}}$ ( $10^3 L_{\odot}$ )	$T_{\text{ex}}$ (K)	$\tau_{13}$	$N(^{13}\text{CO})$ ( $10^{15}$ cm $^{-2}$ )	$N(\text{H}_2)$ ( $10^{21}$ cm $^{-2}$ )	Ref.
IRAS (1)	(2)	(3)	(4)	(5)	(6)	(7)	(8)	(9)	(10)	(11)	(12)	(13)	(14)
00117+6412 <sup>m</sup>	00 14 27.7	+64 28 46	5.72(0.12)	2.55(0.05)	-36.06(0.01)	2.77(0.03)	3.6	4.29	10.50	0.57	5.53	7.87	1N,2,3N,4N,6,7,8
00412+6638	00 44 15.2	+66 54 41	2.64(0.07)	0.81(0.14)	-68.00(0.22)	3.32(0.22)	7.35	15.25	6.96	0.35	3.12	4.44	2N,4
00468+6527	00 49 55.8	+65 43 39	2.31(0.08)	1.17(0.07)	-63.67(0.03)	2.60(0.08)	6.74	34.30	6.55	0.67	4.51	6.42	2,4
00557+5612 <sup>m</sup>	00 58 44.4	+56 28 16	8.37(0.05)	3.72(0.05)	-29.96(0.01)	2.17(0.01)	2.94	1.47 <sup>u</sup>	13.34	0.57	5.84	8.32	11
01134+6429	01 16 48.1	+64 45 37	5.03(0.06) <sup>s</sup>	1.29(0.06)	-54.36(0.02)	2.20(0.06)	3 <sup>a</sup>	1.31	9.73	0.29	2.18	3.10	2,4
02413+6037	02 45 12.5	+60 49 44	2.52(0.06) <sup>s</sup>	0.93(0.04)	-61.56(0.02)	2.22(0.06)	7.47	10.45 <sup>u</sup>	6.81	0.44	2.58	3.68	
02485+6902	02 53 07.2	+69 14 36	4.11(0.04) <sup>s</sup>	1.70(0.05) <sup>s</sup>	-10.52(0.01)	1.94(0.03)	1.09	0.21	8.70	0.51	3.11	4.43	2N
02541+6208	02 58 13.7	+62 20 31	2.28(0.06)	0.59(0.03)	-51.68(0.22)	2.09(0.22)	5.88	6.43 <sup>u</sup>	6.51	0.29	1.55	2.20	2,4
03101+5821 <sup>m</sup>	03 14 04.7	+58 33 08	4.84(0.05)	2.37(0.04)	-38.27(0.01)	2.38(0.02)	4.2	1.20	9.52	0.65	5.03	7.16	2,4N,6
03258+3104 <sup>m</sup>	03 28 56.8	+31 14 44	13.57(0.11)	6.78(0.05)	7.56(0.01)	3.27(0.01)	0.22 <sup>a</sup>	0.03 <sup>u</sup>	18.76	0.68	15.29	21.78	1N
03414+3200 <sup>m</sup>	03 44 36.4	+32 09 25	17.20(0.10)	6.08(0.07)	8.40(0.01)	1.71(0.01)	0.3 <sup>b</sup>	0.05 <sup>u</sup>	22.48	0.43	7.44	10.59	1N,2N
04365+4717	04 40 16.8	+47 23 04	4.06(0.05) <sup>s</sup>	1.65(0.08)	-34.75(0.03)	2.59(0.07)	6.9 <sup>b</sup>	4.37	8.64	0.50	4.04	5.75	2N,4
05155+0707	05 18 17.1	+07 11 01	...	3.34(0.06)	-1.45(0.01)	2.37(0.02)	0.46 <sup>a</sup>	0.03	...	...	...	...	
05168+3634 <sup>m</sup>	05 20 16.2	+36 37 21	3.39(0.06)	2.61(0.09)	-15.18(0.22)	2.43(0.22)	6.08 <sup>c</sup>	17.13	7.86	1.37	14.79	21.05	1N,2N,3,5,6,7,8,10
05221+4139	05 25 39.8	+41 41 50	2.16(0.06)	0.79(0.07)	-25.81(0.05)	2.75(0.13)	10.36	32.75	6.36	0.43	3.05	4.34	2N
05271+3059	05 30 21.2	+31 01 27	2.32(0.07)	0.75(0.06)	-19.73(0.22)	4.36(0.22)	16.5 <sup>b</sup>	72.86	6.56	0.37	4.22	6.01	2
05334+3149	05 36 41.1	+31 51 14	...	1.35(0.06)	-15.98(0.22)	3.77(0.22)	16.5 <sup>b</sup>	97.73	...	...	...	...	2N,3N
05450+0019	05 47 34.6	+00 20 08	6.87(0.09)	3.64(0.07)	9.41(0.22)	4.19(0.22)	0.5 <sup>d</sup>	0.04	11.74	0.73	12.76	18.17	
06067+2138 <sup>m</sup>	06 09 48.0	+21 38 11	...	3.49(0.05)	1.73(0.22)	3.37(0.22)	0.61	0.03 <sup>u</sup>	...	...	...	...	2N,6,10
06103+1523 <sup>m</sup>	06 13 15.1	+15 22 36	6.22(0.07)	2.97(0.09)	15.99(0.02)	3.01(0.04)	3.78	9.49	11.04	0.63	6.91	9.84	1N,2N,3N,6,7,8
06104+1524A	06 13 21.3	+15 23 57	...	3.24(0.19)	16.26(0.03)	2.50(0.07)	3.87	10.59	...	...	...	...	2N,3N,5N,6
06306+0232	06 33 15.8	+02 30 22	...	1.43(0.08)	25.49(0.03)	2.28(0.06)	3.32	0.88	...	...	...	...	
06331+1102	06 35 56.0	+11 00 18	...	2.66(0.10)	22.71(0.22)	2.75(0.22)	3.89	2.58	...	...	...	...	6
06381+1039	06 40 58.0	+10 36 49	9.47(0.19)	2.64(0.10)	7.64(0.02)	2.92(0.05)	1.11	0.20 <sup>u</sup>	14.50	0.32	4.99	7.11	6
06382+1017	06 41 03.3	+10 15 01	7.70(0.08)	3.52(0.09)	7.60(0.01)	2.93(0.04)	1.1	0.17	12.63	0.60	7.88	11.22	
06501+0143	06 52 45.6	+01 40 15	...	1.73(0.07)	45.07(0.02)	2.85(0.05)	6.52	9.44	...	...	...	...	
07024-1102 <sup>m</sup>	07 04 45.7	-11 07 15	...	4.47(0.06)	16.90(0.22)	1.89(0.22)	1.64	0.57	...	...	...	...	6
07111-1211	07 13 29.9	-12 16 51	...	1.22(0.08)	15.71(0.03)	2.37(0.09)	1.53	0.20	...	...	...	...	
07119-1210A	07 14 17.7	-12 15 14	...	2.04(0.10)	15.23(0.03)	2.67(0.06)	1.48	0.23	...	...	...	...	2N
07207-1435	07 23 01.3	-14 41 33	...	1.95(0.13)	53.17(0.04)	2.77(0.09)	5.58	14.50	...	...	...	...	2
17576-1845	18 00 34.3	-18 45 17	...	1.06(0.12)	21.96(0.08)	4.38(0.20)	3.11	1.35	...	...	...	...	
18145-1557	18 17 26.7	-15 56 20	...	1.81(0.20)	25.93(0.07)	4.09(0.19)	2.81	4.07	...	...	...	...	3N
18205-1316	18 23 21.6	-13 15 02	...	2.43(0.12)	22.48(0.22)	2.89(0.22)	2.24	1.52	...	...	...	...	
18236-1241	18 26 24.7	-12 39 37	...	2.07(0.10) <sup>s</sup>	64.57(0.03)	4.33(0.08)	4.6	15.85	...	...	...	...	
18278-0212	18 30 28.0	-02 10 48	...	1.79(0.08)	5.86(0.22)	3.01(0.22)	0.39	0.02	...	...	...	...	

Table 1: continued.

(1)	(2)	(3)	(4)	(5)	(6)	(7)	(8)	(9)	(10)	(11)	(12)	(13)	(14)
18301-0853	18 32 55.2	-08 51 23	...	2.19(0.14)	79.05(0.04)	3.35(0.10)	4.97	13.66	...	...	...	...	
18314-0820	18 34 09.0	-08 17 52	...	4.07(0.08)	105.17(0.22)	4.01(0.22)	6.08	24.52	...	...	...	...	3N
18324-0855	18 35 10.5	-08 52 35	...	0.92(0.10)	3.72(0.03)	0.88(0.09)	0.26	0.03	...	...	...	...	1
18358-0112	18 38 25.9	-01 09 51	...	2.51(0.07)	9.43(0.22)	3.67(0.22)	0.67	0.05	...	...	...	...	
18403-0445	18 38 34.4	-03 32 06	...	1.76(0.10) <sup>s</sup>	45.74(0.03)	3.25(0.08)	3.16	4.66	...	...	...	...	1,6
18502+0033	18 52 47.6	+00 36 51	...	2.33(0.10)	104.90(0.03)	5.26(0.07)	1*	0.50	...	...	...	...	
18502+0034	18 52 50.9	+00 38 03	...	2.40(0.12)	104.70(0.04)	5.55(0.09)	1*	0.52	...	...	...	...	6
18532+0047	18 55 50.6	+00 51 22	...	1.24(0.09) <sup>s</sup>	58.94(0.05)	4.65(0.13)	3.83	8.96	...	...	...	...	3N,8
18545+0202	18 57 02.6	+02 06 23	...	1.45(0.10) <sup>s</sup>	44.87(0.04)	3.68(0.13)	2.99	3.45	...	...	...	...	
18578+0313	19 00 21.1	+03 17 45	...	0.97(0.08) <sup>s</sup>	59.74(0.06)	5.16(0.14)	3.93	3.53	...	...	...	...	
19002+0454	19 02 42.0	+04 58 49	...	1.56(0.13) <sup>s</sup>	68.58(0.06)	3.75(0.15)	4.67	8.71	...	...	...	...	3N,7
19011+0450	19 03 36.9	+04 55 15	...	1.38(0.13)	50.07(0.07)	4.52(0.17)	3.35	4.28	...	...	...	...	
19029+0556	19 05 23.8	+06 01 24	...	2.11(0.13)	58.44(0.22)	4.54(0.22)	3.97	12.65	...	...	...	...	
19031+0621	19 05 36.4	+06 26 09	...	1.65(0.10)	73.36(0.03)	2.38(0.07)	5.41	24.87	...	...	...	...	1
19056+0624	19 08 02.9	+06 29 11	...	1.16(0.12) <sup>s</sup>	66.07(0.06)	3.44(0.17)	4.66	4.51	...	...	...	...	
19205+1358	19 22 53.9	+14 04 11	2.10(0.09)	0.60(0.07)	61.86(0.07)	3.43(0.17)	1*	0.31 <sup>u</sup>	6.28	0.32	2.80	3.99	
19215+1410	19 23 49.4	+14 16 20	...	0.80(0.07)	58.00(0.07)	5.43(0.16)	1*	0.16	...	...	...	...	6N
19216+1658	19 23 52.4	+17 04 01	3.08(0.10)	0.92(0.07)	1.67(0.06)	6.48(0.14)	10.6	62.46 <sup>u</sup>	7.50	0.34	6.18	8.80	
19282+1742	19 30 30.5	+17 48 30	...	2.82(0.08)	61.14(0.22)	2.84(0.22)	1*	0.49	...	...	...	...	3N,6
19286+1722	19 30 54.0	+17 28 46	...	0.88(0.07)	45.48(0.05)	3.24(0.10)	4.78	6.57	...	...	...	...	6
19291+1713	19 31 23.4	+17 19 42	...	1.45(0.07) <sup>s</sup>	48.07(0.03)	3.41(0.07)	1*	0.38	...	...	...	...	
19298+1707	19 32 08.5	+17 13 35	4.97(0.15) <sup>s</sup>	0.87(0.07)	56.61(0.05)	2.64(0.11)	1*	0.19 <sup>u</sup>	9.67	0.19	1.69	2.40	
19348+2229	19 36 59.8	+22 36 08	...	0.82(0.05) <sup>s</sup>	28.48(0.02)	1.31(0.05)	2.66	1.10	...	...	...	...	6N
19368+2239	19 38 58.1	+22 46 32	6.19(0.08) <sup>s</sup>	3.20(0.09)	36.35(0.22)	3.46(0.22)	1*	0.33	11.01	0.70	9.47	13.48	3N,6,7,8
19406+2333	19 42 44.4	+23 40 30	3.03(0.05) <sup>s</sup>	1.06(0.08)	1.01(0.05)	3.56(0.12)	8.74	8.87	7.44	0.41	4.09	5.83	6
19413+2349	19 43 28.3	+23 56 58	9.20(0.16)	3.85(0.09)	22.33(0.01)	1.88(0.03)	2.02	0.60	14.22	0.53	5.19	7.39	6
19415+2312	19 43 39.7	+23 20 06	6.79(0.07)	2.05(0.06)	27.53(0.02)	5.51(0.05)	2.72	2.03 <sup>u</sup>	11.66	0.35	7.97	11.35	6
19560+3135	19 58 03.3	+31 44 07	4.11(0.09)	1.11(0.11)	-65.10(0.22)	2.19(0.22)	13.29	50.84	8.70	0.30	2.08	2.96	3N
19589+3320	20 00 52.6	+33 29 08	7.34(0.10)	1.88(0.08)	-22.51(0.03)	4.78(0.07)	8.44	37.18	12.25	0.29	6.03	8.58	1
20050+2720	20 07 06.7	+27 28 53	3.79(0.08) <sup>s</sup>	2.85(0.11)	6.39(0.02)	4.05(0.06)	0.7 <sup>a</sup>	0.26	8.33	1.31	15.98	22.75	3,7
20062+3550	20 08 09.8	+35 59 20	5.09(0.07)	2.37(0.17)	0.99(0.22)	2.26(0.22)	5.24	18.02	9.80	0.61	4.74	6.74	1,3,6,7,8
20067+3415 <sup>m</sup>	20 08 41.3	+34 24 19	4.40(0.06)	2.64(0.06)	13.68(0.02)	3.62(0.04)	2.36	1.14	9.03	0.88	9.57	13.63	6
20094+2744	20 11 29.1	+27 53 16	...	2.91(0.14)	12.10(0.03)	2.59(0.06)	1.11	0.12	...	...	...	...	
20103+3633	20 12 13.9	+36 42 59	2.53(0.09)	1.70(0.24)	-36.23(0.07)	2.65(0.18)	8.91	29.26	6.83	1.04	7.32	10.42	3N
20116+3605	20 13 33.6	+36 14 55	3.38(0.10) <sup>s</sup>	1.15(0.07) <sup>s</sup>	-53.07(0.03)	2.50(0.07)	10.69	72.70	7.85	0.40	2.89	4.11	
20145+3645	20 16 27.5	+36 54 58	2.70(0.11)	1.10(0.07)	-56.37(0.04)	3.54(0.12)	10.86	50.37	7.04	0.50	4.76	6.78	
20149+3913 <sup>m</sup>	20 16 42.6	+39 23 15	6.91(0.08)	4.61(0.13)	3.82(0.02)	2.97(0.04)	1.7 <sup>f</sup>	0.30 <sup>u</sup>	11.79	1.06	16.85	24.00	6,9
20178+3723	20 19 43.1	+37 33 13	6.03(0.09)	1.96(0.10)	3.93(0.02)	1.84(0.05)	4.08	1.02 <sup>u</sup>	10.83	0.38	2.69	3.83	
20227+4154	20 24 31.4	+42 04 17	7.74(0.08)	3.18(0.12)	5.54(0.02)	2.72(0.05)	2 <sup>a</sup>	2.74	12.68	0.52	6.37	9.06	3,7
20231+3440	20 25 16.0	+34 50 06	3.60(0.07)	1.90(0.14)	5.46(0.04)	2.70(0.09)	1 <sup>a</sup>	0.19	8.11	0.72	5.72	8.14	

Table 1: continued.

(1)	(2)	(3)	(4)	(5)	(6)	(7)	(8)	(9)	(10)	(11)	(12)	(13)	(14)
20261+3922	20 27 58.8	+39 32 07	2.63(0.08) <sup>s</sup>	1.19(0.19)	-54.99(0.09)	2.79(0.20)	10.01	32.70	6.95	0.57	4.28	6.09	
20281+4038	20 29 54.8	+40 48 52	5.50(0.08) <sup>s</sup>	2.05(0.06)	-2.51(0.02)	2.36(0.04)	4.11	6.56	10.25	0.45	3.86	5.50	
20290+4052	20 30 50.8	+41 02 25	3.70(0.08) <sup>s</sup>	1.60(0.10)	-1.51(0.04)	3.15(0.10)	3.89	2.79	8.23	0.54	5.12	7.28	
20326+3757	20 34 33.0	+38 08 02	9.05(0.11)	2.99(0.09)	2.79(0.22)	5.81(0.22)	3.66	2.74 <sup>u</sup>	14.06	0.39	11.72	16.69	
20330+4109	20 34 48.5	+41 20 21	4.07(0.11) <sup>s</sup>	0.67(0.07) <sup>s</sup>	-30.82(0.05)	2.19(0.12)	7.09	10.04 <sup>u</sup>	8.65	0.17	1.19	1.69	
20345+4024	20 36 24.1	+40 35 08	4.12(0.10)	0.82(0.09)	1.31(0.06)	2.58(0.13)	3.34	1.59 <sup>u</sup>	8.71	0.21	1.73	2.47	
20444+4629	20 46 08.3	+46 40 41	6.51(0.09)	3.65(0.07)	-3.71(0.01)	2.09(0.02)	2.91	3.98	11.36	0.80	6.67	9.50	2N,3N,7
20508+4825	20 52 28.2	+48 36 30	1.55(0.05) <sup>s</sup>	0.92(0.07)	-6.63(0.04)	2.58(0.11)	2.98	1.17 <sup>u</sup>	5.55	0.84	5.27	7.51	2N
21025+4912	21 04 15.4	+49 24 25	1.32(0.04) <sup>s</sup>	0.74(0.06)	-73.44(0.05)	2.86(0.12)	10.08	9.15 <sup>u</sup>	5.23	0.76	5.27	7.50	2
21246+5512	21 26 14.4	+55 25 57	0.76(0.05)	0.49(0.06)	-69.33(0.05)	1.84(0.13)	8.72	15.33	4.37	0.93	4.14	5.90	2N
21293+5535	21 30 55.7	+55 48 49	4.42(0.06)	1.17(0.06)	-71.13(0.03)	4.13(0.09)	8.85	8.25 <sup>u</sup>	9.05	0.30	3.97	5.65	2,4
21334+5039	21 35 09.2	+50 53 09	4.64(0.07)	2.36(0.07)	-45.05(0.22)	2.75(0.22)	5 <sup>a</sup>	23.53	9.30	0.68	6.21	8.84	2
21379+5106	21 39 40.8	+51 20 35	2.88(0.07)	1.39(0.07)	-42.27(0.22)	2.17(0.22)	5.9	5.18	7.25	0.63	3.73	5.32	2
21391+5026	21 40 57.3	+50 39 53	2.56(0.07)	1.02(0.07)	-40.55(0.04)	2.50(0.09)	5.77	5.67	6.86	0.48	3.22	4.58	2
21391+5802 <sup>m</sup>	21 40 42.4	+58 16 10	...	5.80(0.07)	0.68(0.01)	2.99(0.02)	0.75 <sup>e</sup>	0.26	...	...	...	...	1N,2N,3,7,8
21418+5403	21 43 29.8	+54 16 56	3.62(0.06)	0.86(0.06)	-60.07(0.04)	3.24(0.10)	7.51	22.24	8.13	0.26	2.51	3.58	2N
21519+5613	21 53 39.2	+56 27 46	4.26(0.06)	2.07(0.08)	-62.72(0.02)	3.11(0.05)	7.3 <sup>a</sup>	15.75	8.87	0.64	6.31	8.98	2,3,4,8
22051+5848	22 06 50.7	+59 02 47	2.40(0.06)	1.51(0.07)	-1.77(0.02)	1.39(0.04)	0.77	0.08 <sup>u</sup>	6.66	0.93	3.38	4.82	2N,4
22198+6336 <sup>m</sup>	22 21 27.6	+63 51 42	10.55(0.01)	5.39(0.07)	-11.10(0.22)	2.65(0.22)	1.67	1.53 <sup>u</sup>	15.63	0.70	11.49	16.36	1N,2N,3,7,8
22305+5803	22 32 24.3	+58 18 58	4.57(0.07)	1.80(0.06)	-52.41(0.02)	2.68(0.05)	5.94	14.28	9.22	0.48	4.25	6.05	2,4,6,8
22506+5944 <sup>m</sup>	22 52 38.6	+60 00 56	11.01(0.07)	3.18(0.05)	-51.61(0.22)	2.43(0.22)	3.5 <sup>d</sup>	6.83	16.11	0.34	5.56	7.92	1N,2N,3,4N,6,7,8,10
22539+5758	22 56 00.0	+58 14 46	7.32(0.06)	3.59(0.07)	-54.19(0.01)	2.97(0.03)	3.5 <sup>d</sup>	10.68	12.23	0.66	8.47	12.07	2,4,5
23011+6126	23 03 13.1	+61 42 26	5.12(0.07)	2.25(0.06)	-11.03(0.22)	1.93(0.22)	0.73 <sup>d</sup>	0.09	9.83	0.56	3.75	5.34	2,4,6

Note.—Column (1) is source name shown in order of ascending *IRAS* number. Columns (2) and (3) list J2000 equatorial coordinates of each source. Column (4) lists the main beam temperature of  $^{12}\text{CO } J=2-1$  if available, and Cols. (5)–(7) list the main beam temperature, local standard of rest velocity and line width of  $^{13}\text{CO } J=2-1$ , with  $1\sigma$  rms level in parenthesis. Column (8) is kinematic distance except for otherwise labeled. Column (9) lists the bolometric luminosity with asterisk (\*) if one (or two) *IRAS* band flux is upper limit. Column (10) is excitation temperature. Column (11) is the opacity of  $^{13}\text{CO}$ . Columns (12)–(13) present average  $^{13}\text{CO}$  and  $\text{H}_2$  column densities. Column (14) lists former works if available.

References.— (1) 6.7 GHz methanol maser survey (Szymczak et al., 2000); (2) 22 GHz water maser survey (Wouterloot et al., 1993); (3) 22 GHz water maser (Palla et al., 1991); (4) 1665/67 MHz OH maser survey (Wouterloot et al., 1993); (5)  $\text{HCO}^+ J=1-0$  survey (Richards et al., 1987); (6)  $\text{CS } J=2-1$  survey (Bronfman et al., 1996); (7)  $\text{NH}_3 (J,K)=(1,1) (2,2)$  survey (Molinari et al., 1996); (8)  $\text{CO } J=2-1$  outflow mapping (Zhang et al., 2005; Kim & Kurtz, 2006); (9)  $\text{CO}$ ,  $\text{CS}$  mapping (Ao et al., 2004); (10)  $\text{CO}$  mapping (Guan et al., 2008); (11)  $\text{CO}$  mapping (Lee & Jung, 2003). N means non-detection.

<sup>a-f</sup> distance from <sup>a</sup> Wu et al. (2004), <sup>b</sup> Wouterloot et al. (1993), <sup>c</sup> Molinari et al. (1996), <sup>d</sup> Harju et al. (1993), <sup>e</sup> Matthews (1979), <sup>f</sup> Motte et al. (2007);

\* kinematic distance unavailable, set as 1 kpc;

<sup>m</sup> mapped source;

<sup>s</sup> more than one velocity component, only the strongest one listed;

<sup>u</sup> upper limit.